Thermal quenching of Ce^{3+} emission in PrX_3 (X = Cl, Br) by intervalence charge transfer

2007 J. Phys.: Condens. Matter 19 256209

(http://iopscience.iop.org/0953-8984/19/25/256209)

J. Phys.: Condens. Matter **19** (2007) 256209 (16pp) doi:10.1088/0953-8984/19/25/256209

Thermal quenching of Ce^{3+} emission in PrX_3 (X = Cl, Br) by intervalence charge transfer

M D Birowosuto[1], P Dorenbos[1], C W E van Eijk[1], K W Krämer[2] and H U Güdel[2]

[1] Radiation Detection and Matter, Department of Applied Sciences, Delft University of Technology, Mekelweg 15, 2629 JB, Delft, The Netherlands
[2] Department of Chemistry and Biochemistry, University of Bern, Freiestrasse 3, 3000 Bern 9, Switzerland

E-mail: M.D.Birowosuto@tnw.tudelft.nl and P.Dorenbos@tnw.tudelft.nl

Received 4 April 2007, in final form 17 May 2007
Published 5 June 2007
Online at stacks.iop.org/JPhysCM/19/256209

Abstract

The cause of the relatively low scintillation light yield of $PrBr_3$:Ce^{3+} is investigated by means of optical spectroscopy, the temperature dependence of scintillation properties and the temperature dependence of optically excited decay curves of undoped and Ce^{3+}-doped $PrCl_3$ and $PrBr_3$. The integrated intensity of x-ray excited luminescence of $PrBr_3$:5% Ce^{3+} shows that the light yield at room temperature (RT) is two times less than at 80 K. The decay time of Ce^{3+} emission optically excited to its 5d band in $PrBr_3$:5% Ce^{3+} has a single exponential decay of 11.0 ± 1.1 and 6.0 ± 0.6 ns at 10 K and RT, respectively. It is proposed that Ce^{3+} emission is quenched by a metal-to-metal charge transfer of $Ce^{3+} + Pr^{3+} \rightarrow Ce^{4+} + Pr^{2+}$ followed by 4f $\rightarrow$ 4f emission of Pr^{3+} which is strongly concentration quenched.

1. Introduction

There is a continued interest in the search for new scintillators for the detection of radiation. Much effort has already been devoted to the Ce^{3+}-doped lanthanide trihalide family. Among all investigated compounds, $LaCl_3$:Ce^{3+}, $LaBr_3$:Ce^{3+} and LuI_3:Ce^{3+} show outstanding scintillation properties including high light yield, good energy resolution and fast decay time [1–3].

Besides Ce^{3+}, there are also efforts to introduce the Pr^{3+} ion as an optically active dopant [4]. Theoretically, the 5d $\rightarrow$ 4f emission in Pr^{3+} should be a factor of two to three faster than in Ce^{3+} due to the higher energy of the 5d $\rightarrow$ 4f emission of Pr^{3+} compared to Ce^{3+} [5]. Unfortunately, developing $LaBr_3$:Pr^{3+} as a new fast scintillator has not been successful. It does not show the anticipated 5d $\rightarrow$ 4f emission; instead, slow 4f $\rightarrow$ 4f emission is observed. The

charge transfer (CT) from the valence band to Pr^{3+} occurs at an energy below the energy of the 5d $\rightarrow$ 4f emission, and this quenches Pr^{3+} emission [6].

Recently, Nikl *et al* investigated the scintillation characteristics of PrF_3:Ce^{3+} [7]. This was the first scintillation study on a Ce^{3+}-doped praseodymium host. In PrF_3:Ce^{3+}, the energy transfer from the Pr^{3+} host to the Ce^{3+} via the $^1S_0$ level of Pr^{3+} is efficient and Ce^{3+} doping can be accomplished at an arbitrary level because PrF_3 and CeF_3 are isostructural [7]. We decided to study the scintillation properties of Ce^{3+}-doped $PrCl_3$ and $PrBr_3$ [8]. Undoped $PrCl_3$ and $PrBr_3$ were previously studied for surface laser applications [9]. Studies of radiative and nonradiative transitions of Pr^{3+} in undoped $PrCl_3$ and $PrBr_3$ can be found in the works of German *et al* [10, 11].

We previously reported a scintillation light yield of $PrBr_3$:Ce^{3+} up to 21 000 photons MeV^{-1} [8]. This is three and a half times less than that of $LaBr_3$:Ce^{3+}. The cause of the relatively low scintillation light yield in $PrBr_3$:Ce^{3+} is interesting to investigate. In this work, optical spectroscopy, x-ray excited luminescence spectra and pulse height spectra as a function of temperature are presented in order to study the thermal quenching behaviour. A thermal quenching model is then proposed. Scintillation and optical properties of Ce^{3+}-doped $PrCl_3$ are also presented.

2. Experimental procedures

2.1. Crystal growth and structure

Crystals of undoped and 5% Ce^{3+}-doped $PrCl_3$ and $PrBr_3$ of $5 \times 3 \times 2$ mm^3 were grown using the Bridgman technique. Starting materials of PrX_3 and CeX_3 (X = Cl, Br) were prepared from Pr_6O_{11} (Ultrafunction enterprise, 5N5), CeO_2 (Ultrafunction enterprise, 6N), NH_4X (X = Cl, Br) (Merck, 99.9%), and HX (X = Cl, Br) (47% Merck, suprapur) by the ammonium halide method [12]. For the crystal growth, stoichiometric amounts of starting materials were sealed in silica ampoules under vacuum.

$PrCl_3$ and $PrBr_3$ show the UCl_3-type structure with space group $P6_3/m$ (no. 176) [13]. The structure can also be described as a hexagonal close packed arrangement of chains of edge-connected polyhedra (PrX_9). The polyhedron can be viewed as a tricapped trigonal prism with the Pr^{3+} ion in the centre. The nine Cl^- or Br^- ions are at an average distance of 292 or 307 pm from the central Pr^{3+} ion, respectively. The calculated densities of $PrCl_3$ and $PrBr_3$ are 4.02 and 5.33 g cm^{-3}, respectively, which is slightly larger than those of $LaCl_3$ (3.86 g cm^{-3}) and $LaBr_3$ (5.07 g cm^{-3}) [1, 2].

2.2. Experimental techniques

X-ray excited luminescence spectra were excited with an x-ray tube with a Cu anode operating at 35 kV and 25 mA. The emission of the sample was dispersed by means of an Acton Research Corporation (ARC) VM-504 monochromator (blazed at 300 nm, 1200 grooves nm^{-1}) and detected by a Hamamatsu R934-04 Photomultiplier Tube (PMT). The spectra in this study were corrected for the wavelength dependence of the photodetector quantum efficiency as well as monochromator transmission. Temperature-dependent x-ray excited emission measurements were performed between 80 and 600 K, using a JANIS VPF-700 Cryostat operated with a Model 331 LakeShore Temperature Controller.

The light yield at RT was determined from the 662 keV total absorption peak in the pulse height spectrum of a ^{137}Cs source detected with the scintillation crystal mounted directly on a Hamamatsu R1791 PMT recorded with 0.5 and 10 μs shaping times. The yield, expressed

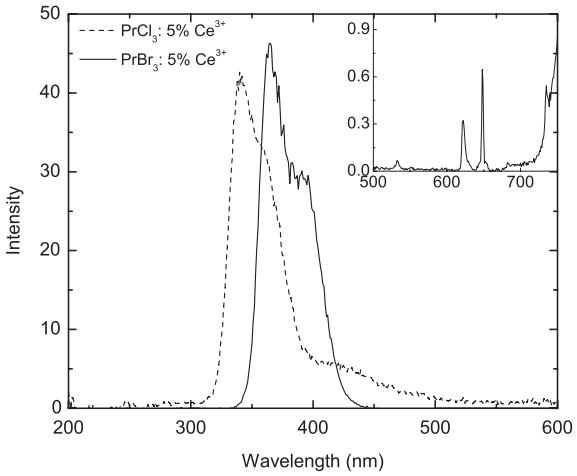

Figure 1. X-ray excited emission spectra of $PrCl_3$:5% Ce^{3+} and $PrBr_3$:5% Ce^{3+} at RT. The inset shows the x-ray excited emission spectrum of $PrBr_3$:5% Ce^{3+} between 500 and 750 nm on a 20 times enlarged scale. The increase in the intensity above 700 nm is due to second-order transmission.

in photoelectrons per MeV of absorbed γ-ray energy (phe MeV^{-1}), was determined by comparison of the total γ-ray energy absorption peak with the single photoelectron peak. The light yield expressed in photons per MeV (photons MeV^{-1}) is determined using the quantum efficiency and reflectivity of the PMT [14].

Scintillation decay curves under ^{137}Cs 662 keV γ-ray excitation were recorded at RT by the conventional delayed coincidence method described by Bollinger and Thomas [15]. For this method, scintillation decay time curves were recorded at timescales up to 200 μs using Philips XP2020Q PMTs, Ortec 934 Constant Fraction Discriminators, an Ortec 567 Time to Analog Converter (TAC) and an AD413A CAMAC Analog to Digital Converter (ADC).

Time-resolved excitation and emission spectra at 10 and 300 K were recorded using synchrotron radiation at the SUPERLUMI station of the Synchrotron Strahlungslabor (HASYLAB) at the Deutches Electronen Synchrotron (DESY) in Hamburg (Germany). Details of this setup have been described elsewhere [16, 17].

Decay curves with selected excitation and emission wavelengths were recorded using a Model 5000 IBH coaxial flash lamp. The lamp was filled with hydrogen gas and operated at 7.0 keV and a frequency of 40 kHz. The excitation wavelength was dispersed using an ARC VM502 monochromator. The emission of the sample was selected using either the band or cutoff filters and detected by a Hamamatsu R934-04 PMT. Decay curves were obtained after deconvolution with the function of the system response. Temperature-dependent decay curves were recorded with the same cryostat and temperature controller as those of temperature-dependent x-ray excited luminescence spectra, whereas the setup of temperature-dependent γ-excited pulse height spectra is described in [18].

3. Results

3.1. Scintillation properties

X-ray excited emission spectra of $PrCl_3$:5% Ce^{3+} and $PrBr_3$:5% Ce^{3+} at RT are shown in figure 1. For both compounds, characteristic Ce^{3+} 5d $\rightarrow$ 4f emission is observed. The maxima

Table 1. Scintillation light yields of $PrCl_3$:5% Ce^{3+} and $PrBr_3$:5% Ce^{3+} under 662 keV γ-ray excitation. Those of $LaCl_3$:4% Ce^{3+} and $LaBr_3$:5% Ce^{3+} are added for comparison. Light yields were measured with 0.5 and 10 μs shaping times.

	Light yield (photons MeV^{-1}) $^{137}Cs\gamma$-rays (RT)		
Compounds	0.5 μs	10 μs	Reference
$PrCl_3$:5% Ce^{3+}	18 500 ± 1900	20 500 ± 2100	This work
$LaCl_3$:4% Ce^{3+}	37 000 ± 3700	49 000 ± 4900	[19]
$PrBr_3$:5% Ce^{3+}	14 500 ± 1500	16 000 ± 1600	[8]
$LaBr_3$:5% Ce^{3+}	67 000 ± 6700	67 000 ± 6700	[2]

are located at 340 and 365 nm for the chloride and at 366 and 395 nm for the bromide for the 5d $\rightarrow$ $^2F_{5/2}$ and $^2F_{7/2}$ transitions, respectively. Additionally, a broadband or a tail on the long-wavelength side of the Ce^{3+} doublet is present in the x-ray excited emission spectrum of $PrCl_3$:5% Ce^{3+}. Similar bands were observed for $LaCl_3$:Ce^{3+} and K_2LaX_5:Ce^{3+} (X = Cl, Br, I) [19, 20]. We attribute this band to self-trapped exciton (STE) emission. This emission is not observed in the x-ray excited emission spectrum of $PrBr_3$:5% Ce^{3+}. The STE emission was also not observed for $LaBr_3$:5% Ce^{3+} [20]. Pr^{3+} $4f^2 \rightarrow 4f^2$ emission lines are present in the spectrum of $PrBr_3$:5% Ce^{3+}; see the inset in figure 1. These lines are not seen in the x-ray excited emission spectrum of $PrCl_3$:5% Ce^{3+}.

Table 1 shows scintillation light yields derived from the pulse height spectra of $PrCl_3$:5% Ce^{3+} and $PrBr_3$:5% Ce^{3+} at RT. The light yields of $PrCl_3$:5% Ce^{3+} and $PrBr_3$:5% Ce^{3+} are 42% and 24% of that of $LaCl_3$:4% Ce^{3+} and $LaBr_3$:5% Ce^{3+}, respectively [19, 2]; see column 3 in table 1.

Scintillation decay time curves of (a) $PrCl_3$:5% Ce^{3+}, (b) $LaCl_3$:4% Ce^{3+}, (c) $PrBr_3$:5% Ce^{3+} and (d) $LaBr_3$:5% Ce^{3+} at RT are shown in figure 2. The $PrCl_3$:5% Ce^{3+} decay curve was fitted with two exponential decay components of 17 ± 2 and 230 ± 20 ns with the contributions to the total light yield of 80 and 20%, respectively. The three decay components of $LaCl_3$:4% Ce^{3+} are 25 ± 3, 210 ± 20, and 1100 ± 100 ns with contributions to the total light yield of 18%, 25%, and 57%, respectively [19]. The fit of the $PrBr_3$:5% Ce^{3+} decay curve was already presented in Birowosuto *et al* [8]. For $PrBr_3$:5% Ce^{3+}, three decay processes were proposed. They are direct processes with a decay time constant of 6 ns and two delayed processes with transfer time constants of 1 and 9 ns [8]. The decay time constant of the direct process of 6 ns in [8] is faster than that of 16 ns for $LaBr_3$:5% Ce^{3+} reported by Bizarri *et al* [18].

3.2. Luminescence characteristics

The excitation spectra of $PrCl_3$:5% Ce^{3+}, 5% Ce^{3+}-doped and undoped $LaCl_3$, 5% Ce^{3+}-doped and undoped $PrBr_3$, $LaBr_3$:5%Ce^{3+} and $LaBr_3$:0.5% Pr^{3+} recorded at 10 K are shown in figure 3. The excitation spectrum of $PrCl_3$:5% Ce^{3+} monitoring Ce^{3+} emission at 336 nm shows several bands between 210 and 300 nm in spectrum (a) in figure 3. The bands between 230 and 290 nm in spectrum (a) in figure 3 are assigned to the interconfigurational Ce^{3+} [Xe] $4f^1 \rightarrow$ [Xe] $5d^1$ excitations. Compared with the excitation spectrum of $LaCl_3$:5% Ce^{3+} monitoring Ce^{3+} emission at 350 nm in spectrum (c) in figure 3, the highest-energy 5d band of Ce^{3+} in $PrCl_3$:5% Ce^{3+} is shifted 5 nm to longer wavelength. The 5d bands of Ce^{3+} in $LaCl_3$:5% Ce^{3+} were previously identified by Guillot-Noël *et al* [1].

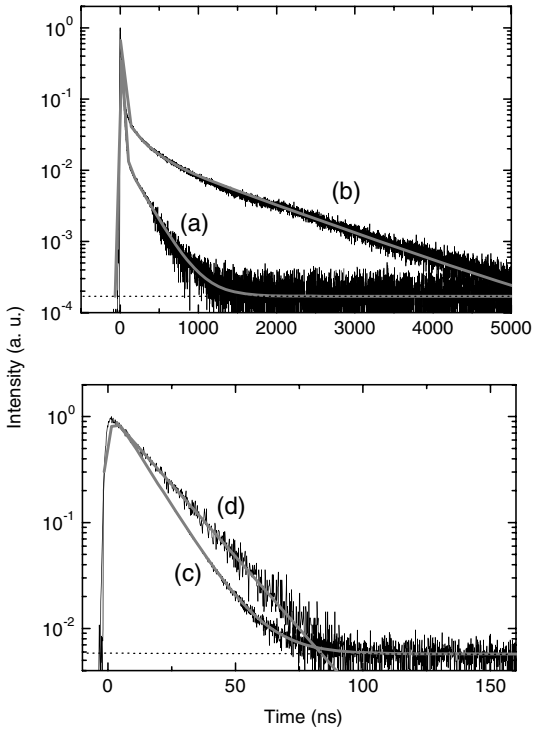

Figure 2. Scintillation decay curves of (a) $PrCl_3$:5% Ce^{3+}, (b) $LaCl_3$:4% Ce^{3+}, (c) $PrBr_3$:5% Ce^{3+} and (d) $LaBr_3$:5% Ce^{3+} at RT. The solid lines through the data and the dotted lines are the exponential fits and the corresponding background levels from each curve.

One band at 216 nm in spectrum (a) in figure 3 also appears in the excitation spectrum when monitoring the $^3P_0 \rightarrow {}^3H_4$ transition line of Pr^{3+} at 490 nm; see the spectrum (b) in figure 3. This band is attributed to the lowest 4f $\rightarrow$ 5d excitation of Pr^{3+} [21]. Empirically, the energy of the lowest 4f $\rightarrow$ 5d transition of Pr^{3+} can be estimated from the lowest 4f $\rightarrow$ 5d transition of Ce^{3+} using [22].

$$E[Pr^{3+}, 4f \rightarrow 5d_{lowest}] = E[Ce^{3+}, 4f \rightarrow 5d_{lowest}] + 1.52 \pm 0.09\ \text{eV}. \quad (1)$$

From spectrum (a) in figure 3, the 4f $\rightarrow 5d_{lowest}$ transition of Ce^{3+} is located at 290 nm (4.28 eV). Then, the 4f $\rightarrow 5d_{lowest}$ transition of Pr^{3+} is expected at 214 $\pm$ 3 nm (5.80 $\pm$ 0.09 eV). This value agrees with the maximum at 216 nm in the excitation spectrum monitoring 490 nm emission; see spectrum (b) in figure 3. Additionally, a tail band between 160 and 206 nm is observed in the excitation spectrum monitoring 336 nm emission; see spectrum (a) in figure 3. This band can be attributed to host lattice excitation from the valence to conduction bands. In undoped $LaCl_3$, the maximum of this host lattice excitation band was observed at 190 nm (6.53 eV); see spectrum (d) in figure 3.

The excitation spectrum of undoped $PrBr_3$ monitoring the $^3P_0 \rightarrow {}^3H_4$ line emission of Pr^{3+} at 490 nm shows the host lattice excitation from valence to conduction bands; see spectrum (e) in figure 3. The fundamental absorption (E_{fa}) at 217 nm (5.71 eV) is defined as the energy of the first sharp onset in the excitation spectra monitoring intrinsic emission. The first maximum (E_{ex}) at 205 nm (6.05 eV) is tentatively attributed to the creation of excitons which can be regarded as bound electron–hole pairs. The edge of the conduction band (E_{VC})

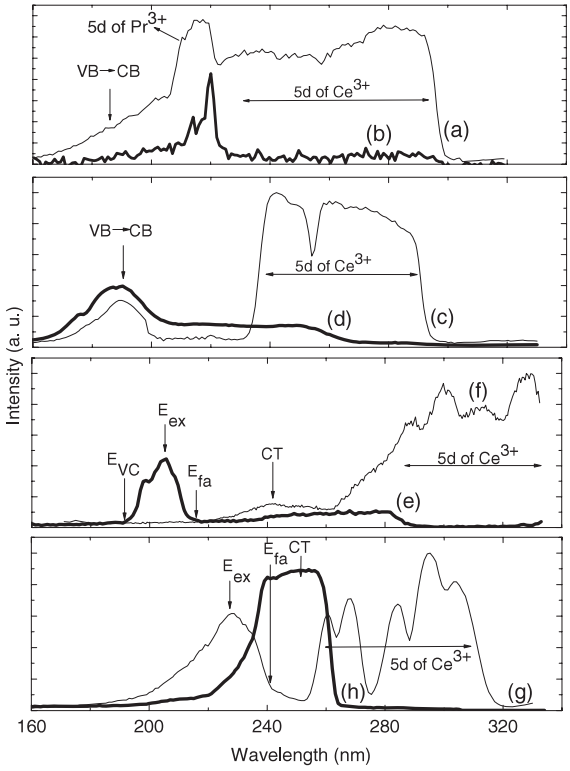

Figure 3. Excitation spectra of $PrCl_3$:5% Ce^{3+} monitoring (a) 336 and (b) 490 nm emission, (c) $LaCl_3$:5% Ce^{3+} monitoring 350 nm emission, (d) undoped $LaCl_3$ monitoring 400 nm emission, (e) undoped $PrBr_3$ monitoring 490 nm emission, (f) $PrBr_3$:5% Ce^{3+} monitoring 380 nm emission, (g) $LaBr_3$:5% Ce^{3+} monitoring 365 nm emission, and (h) $LaBr_3$:0.5% Pr^{3+} monitoring 535 nm emission. All spectra were recorded at 10 K.

estimated at 191 nm (6.50 eV) corresponds to the creation of free electrons in the conduction band and free holes in the valence band. This estimation is based on our assumption that the binding energy of the electron and hole pair in an exciton is about 8% of the exciton creation energy [23].

E_{fa}, E_{ex}, and E_{VC} in undoped $LaBr_3$ were previously reported by Dorenbos *et al* [6]. These energies can also be derived from spectrum (g) in figure 3. When we compare with spectrum (e) in figure 3, E_{fa}, E_{ex}, and E_{VC} in undoped $PrBr_3$ are 0.59 ± 0.06 eV shifted to higher energy than those in undoped $LaBr_3$.

The excitation spectrum of $PrBr_3$:5% Ce^{3+} monitoring Ce^{3+} emission at 380 nm shows several bands between 220 and 330 nm; see spectrum (f) in figure 3. Some bands at wavelengths above 260 nm are assigned to interconfigurational Ce^{3+} $[Xe]\ 4f^1 \rightarrow [Xe]\ 5d^1$ transitions. They are at ≈277 (tentative), 288, 299, 312, and 328 nm. The 5d bands of Ce^{3+} in $PrBr_3$:Ce^{3+} are shifted to longer wavelengths compared to those in $LaBr_3$:Ce^{3+}; see spectrum (g) in figure 3. We obtain energies for the total 5d Ce^{3+} crystal field splitting and the 5d Ce^{3+} centroid shift in $PrBr_3$:Ce^{3+} of 0.70 and 2.22 eV, respectively. The total 5d Ce^{3+} crystal field splitting and the 5d Ce^{3+} centroid shift are the energy difference between the highest and the lowest 5d Ce^{3+} levels and the lowering of the average position of the 5d Ce^{3+} levels in the crystal relative to the position in the free ion, respectively [24]. Both are due to the

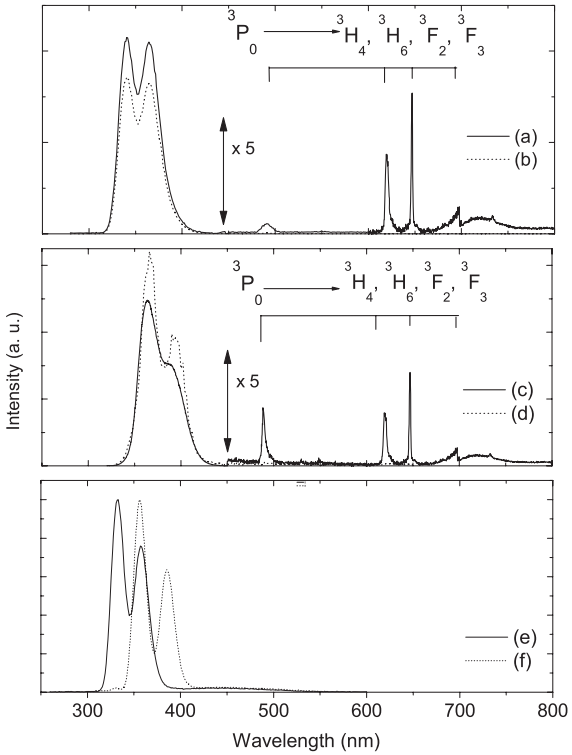

Figure 4. Emission spectra of $PrCl_3$:5% Ce^{3+} excited at (a) 216 and (b) 280 nm recorded at 10 K, $PrBr_3$:5% Ce^{3+} excited at 285 nm recorded at (c) RT and (d) 10 K, (e) $LaCl_3$:4% Ce^{3+} excited at 245 nm recorded at 10 K, and (f) $LaBr_3$:5% Ce^{3+} excited at 295 nm recorded at 10 K. The spectra (a)–(d) between 450 and 800 nm are enlarged by a factor of five.

interaction with the crystalline environment. The energy for the total 5d Ce^{3+} crystal field splitting for $PrBr_3$:Ce^{3+} is almost identical with the 0.74 eV observed for $LaBr_3$:Ce^{3+}, whereas the energy for the 5d Ce^{3+} centroid shift for $PrBr_3$:Ce^{3+} is larger compared to the 1.97 eV for $LaBr_3$:Ce^{3+} [6].

A band at 240 nm (5.17 eV) in spectrum (f) in figure 3 is also observed in $LaBr_3$:Pr^{3+} when monitoring the $^3P_1 \rightarrow {}^3H_5$ line emission of Pr^{3+} at 535 nm; see spectrum (h) in figure 3. This band is attributed to a valence band (VB) $\rightarrow$ Pr^{3+} CT transition [6]. The lowest 4f $\rightarrow$ 5d transition of Pr^{3+} in $PrBr_3$:Ce^{3+} can be estimated from the lowest 4f $\rightarrow$ 5d transition of Ce^{3+} using equation (1). It is expected at 234 $\pm$ 4 nm (5.30 $\pm$ 0.09 eV).

The emission spectra of $PrCl_3$:5% Ce^{3+} and $PrBr_3$:5% Ce^{3+} recorded at 10 K and RT are shown in figure 4. All spectra show two overlapping bands peaking at 340 and 365 nm and 366 and 395 nm for $PrCl_3$:5% Ce^{3+} and $PrBr_3$:5% Ce^{3+}, respectively. These bands are attributed to transitions from the lowest 5d level to $^2F_{5/2}$ and $^2F_{7/2}$ levels of Ce^{3+}, which were also observed in the x-ray excited emission spectra of figure 1. This emission of $PrCl_3$:5% Ce^{3+} and $PrBr_3$:5% Ce^{3+} is shifted by 8 and 10 nm to longer wavelengths compared to that of $LaCl_3$:4% Ce^{3+} and $LaBr_3$:5% Ce^{3+}, respectively; see spectra (e) and (f) in figure 4. Pr^{3+} 4f $\rightarrow$ 4f emission lines are also present and originate from the $^3P_0$ state. These emission lines were previously observed by German and co-workers [11]. They attributed the absence of the emission from the $^3P_1$ state to the energy exchange with neighbouring Pr^{3+} ions [11].

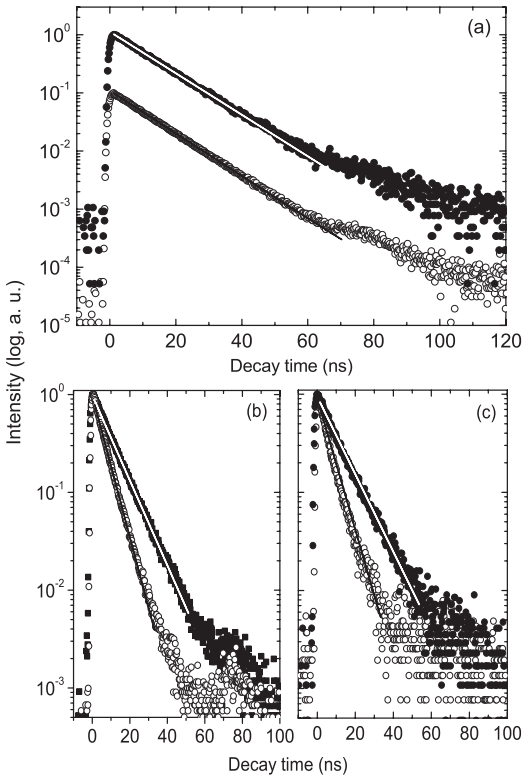

Figure 5. Decay curves of (a) $PrCl_3$:5% Ce^{3+} excited via the 5d band of Ce^{3+} at 280 nm monitoring 336 nm emission, and $PrBr_3$:5% Ce^{3+} excited via (b) the 5d band of Ce^{3+} at 300 nm and (c) the CT band of Pr^{3+} at 240 nm monitoring 366 nm emission. Decay curves with filled circles (•) were recorded at 10 K, whereas those with empty circles (○) were recorded at RT. Solid lines through the data are single exponential fits.

The emission spectra of $PrCl_3$:5% Ce^{3+} recorded at 10 K show that the Pr^{3+} 4f → 4f lines appear only when we excite the 4f → 5d transition of Pr^{3+} at 216 nm; see spectrum (a) in figure 4. This excitation is transferred to Ce^{3+} since we also observe the Ce^{3+} doublet emission. The emission spectrum of $PrBr_3$:5% Ce^{3+} excited via the 5d band of Ce^{3+} at 285 nm recorded at RT shows the Pr^{3+}4f → 4f lines, whereas that recorded at 10 K does not show the Pr^{3+} 4f → 4f lines; see spectra (c) and (d) in figure 4. This means that there is a transfer from Ce^{3+} to the $^3P_0$ state of Pr^{3+} at RT but not at 10 K.

Figure 5 shows decay curves of Ce^{3+} emission with different excitation of $PrCl_3$:5% Ce^{3+} and $PrBr_3$:5% Ce^{3+} recorded at 10 K and RT. All decay curves were fitted with a single exponential decay. Decay curves of the $5d_1$ excited state of Ce^{3+} in $PrCl_3$:5% Ce^{3+} both recorded at 10 K and RT show a decay time of 12.0 ± 2.0 ns; see curves (a) in figure 5. This decay time is faster than the 16 ns decay time of the 5d→ 4f emission of Ce^{3+} in $LaCl_3$:Ce^{3+} [25]. Decay curves of $PrBr_3$:5% Ce^{3+} show identical decay times when excited via the Ce^{3+} 5d band and the CT band of Pr^{3+}; see curves (b) and (c) in figure 5. Unlike the decay curves of $PrCl_3$:5% Ce^{3+}, the decay curves of $PrBr_3$:5% Ce^{3+} are temperature dependent. The decay times are 11.0 ± 1.1 and 6.0 ± 0.6 ns at 10 K and RT, respectively. This indicates the presence of thermal quenching of Ce^{3+} emission. The decay time at 10 K is still faster than the 15 ns decay time of the 5d excited state of Ce^{3+} in $LaBr_3$:Ce^{3+} [18].

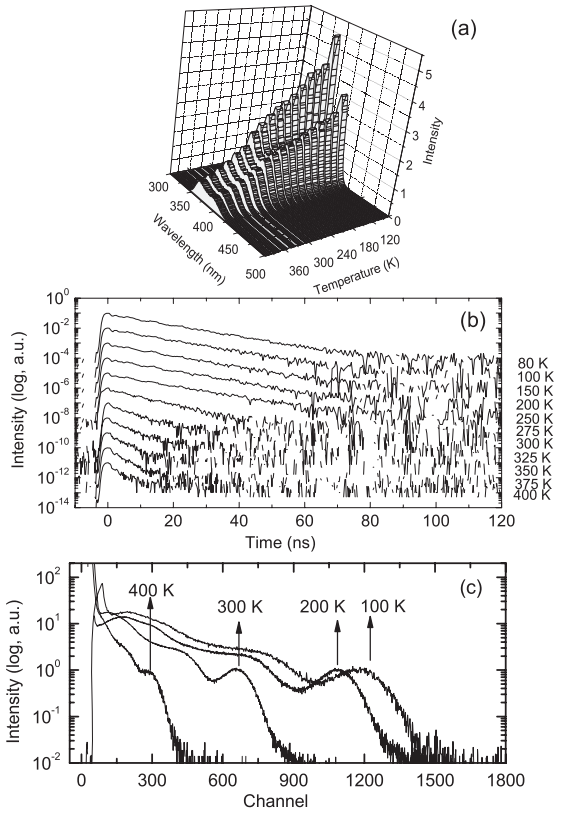

Figure 6. Temperature dependence of (a) x-ray excited emission spectra, (b) decay curves of the 360 nm emission excited via the 5d band of Ce^{3+} at 280 nm, and (c) pulse height spectra under 662 keV γ-ray excitation from ^{137}Cs source recorded with 10 μs shaping time of $PrBr_3$:5% Ce^{3+}.

3.3. Temperature dependence

Figure 6(a) exhibits the x-ray excited emission spectra recorded between 300 and 500 nm, whereas figures 6(b) and (c) show the decay curves optically excited at the 5d state of Ce^{3+} and the γ-excited pulse height spectra recorded with 10 μs shaping time as a function of temperature of $PrBr_3$:5% Ce^{3+}, respectively. The Ce^{3+} x-ray excited emission intensity decreases from 80 to 400 K. This is accompanied by a shortening of the decay time of the Ce^{3+} emission and a shift of the 662 keV photopeaks in the pulse height spectra towards lower channels. The corresponding photopeak position for each temperature is shown by the arrows; see figure 6(c). In order to analyse this Ce^{3+} luminescence quenching, the integral of the x-ray excited emission spectra recorded between 300 and 500 nm, the decay time of Ce^{3+} emission, and the light yields derived from the pulse height spectra as a function of temperature are shown in figure 7. All data exhibit the same type of thermal quenching behaviour.

The dotted curves through the data in figure 7 are model calculations. The integral of the x-ray excited emission spectra and the light yield of the luminescence are given by

$$I(T) = \frac{I_0}{1 + \Gamma_0/\Gamma_v \exp(-\Delta E_q/kT)} \tag{2}$$

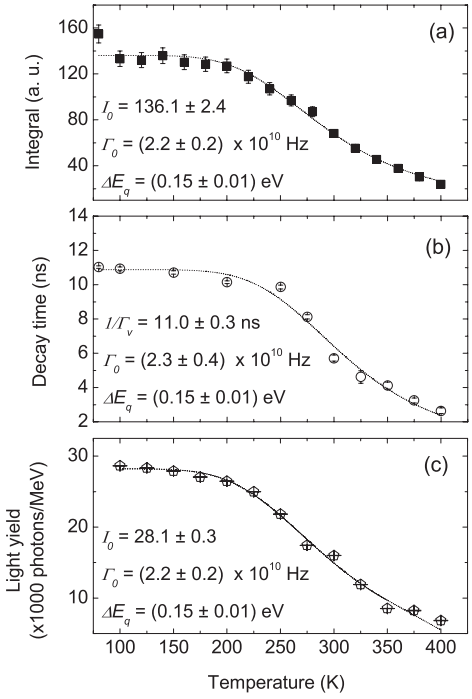

Figure 7. Temperature dependence of (a) the integral of the x-ray excited emission spectra recorded between 300 and 500 nm, (b) the decay time of Ce^{3+} emission and (c) scintillation yields of $PrBr_3$:5% Ce^{3+}. All data were derived from figure 6. The dotted lines through the data are model curves.

and the decay time is given by

$$\tau(T) = \frac{1/\Gamma_v}{1 + \Gamma_0/\Gamma_v \exp(-\Delta E_q/kT)} \tag{3}$$

where $I(T)$ and $\tau(T)$ are the integral of the light yield and the decay time at temperature T, respectively. I_0 is the integral of the light yield at $T = 0$ K. Γ_0 and Γ_v, respectively, are the thermal quenching rate at $T = \infty$ (attempt rate) and the radiative Ce^{3+} 5d $\rightarrow$ 4f transition rate. ΔE_q is the activation energy for thermal quenching and k is the Boltzmann constant. From a fit to equations (2) and (3), fitting parameters are presented in figure 7. The thermal activation energy (ΔE_q) is around 0.15 eV for all temperature-dependence measurements. The radiative lifetime of Ce^{3+} 5d $\rightarrow$ 4f transition ($1/\Gamma_v$) of 11.0 $\pm$ 0.3 ns and the light yield at $T = 0$ K (I_0) of 28 100 $\pm$ 300 photons MeV^{-1} were obtained. Similar values of the attempt rate (Γ_0) are derived from the values of Γ_0/Γ_v found in equations (2) and (3). These attempt rates are in the order of 10^{10} Hz.

4. Discussion

The lifetime of the Ce^{3+} 5d state in compounds can be determined by different processes. First we have the spontaneous radiative lifetime of the 5d state determined by the oscillator strength. In addition, thermally excited interconfigurational system crossing from 5d to 4f or thermally excited 5d to conduction band ionization processes may occur. Lifetime shortening by means of energy transfer to neighbouring acceptor sites may also take place.

Table 2. Summary of the radiative decay parameter for Ce^{3+} in REX_3 (RE = La, Pr and X = Cl, Br). Values in brackets are the estimated values.

Host	τ_r (ns)	λ (nm)	$\lvert\langle 5d\rvert r\rvert 4f\rangle\rvert_{eff}$ (nm)	n	Reference
$LaCl_3$	16	332	0.031	1.80	[31]
$LaBr_3$	15	356	0.031	1.95	[31]
$PrCl_3$	12	340	(0.022–0.034)	(2.38–1.89)	This work
$PrBr_3$	11	366	(0.022–0.034)	(2.57–2.06)	This work

We have observed that the Ce^{3+} decay times excited via the 5d state at 10 K of $PrCl_3$:Ce^{3+} and $PrBr_3$:Ce^{3+} are 11 and 12 ns, respectively. They are 4 ns faster than those of $LaCl_3$:Ce^{3+} and $LaBr_3$:Ce^{3+}, which are 15 and 16 ns, respectively. In part 1, we will discuss the possible causes of this reduced lifetime. In part 2, we will discuss the thermal quenching of Ce^{3+} emission and, based on energy-level schemes derived in part 3, we will propose a new mechanism of 5d $\rightarrow$ 4f emission quenching for Ce^{3+} in Pr-based compounds in part 4.

4.1. Radiative lifetimes of Ce^{3+} in $PrCl_3$:Ce^{3+} and $PrBr_3$:Ce^{3+}

In this part of the discussion, we will attend to explaining the faster radiative lifetimes of the Ce^{3+} 5d $\rightarrow$ 4f transition in PrX_3:Ce^{3+} (X = Cl, Br) compared to those of LaX_3:Ce^{3+} (X = Cl, Br) by means of the spontaneous radiative emission rate.

The spontaneous radiative emission rate Γ_r of the electric dipole transition from a localized initial state $\langle i|$ to a localized final state $|f\rangle$ can be written as [26]

$$\Gamma_r = \frac{64\pi^4}{3h}\chi v_{if}^3 |\langle i| - e\vec{r}|f\rangle|^2 \tag{4}$$

where h is the Planck constant, v_{if} is the emission wavenumber, $-e\vec{r}$ is the electric dipole moment between state $\langle i|$ and $|f\rangle$, and χ is an enhancement factor due to the dielectric medium. However, two models predict substantially different dependences of χ on the refractive index n. They are the virtual- and real-cavity models [27]. Recently, Duan *et al* investigated the radiative lifetimes of Ce^{3+} in different hosts and found that the observed dependence of the Ce^{3+} decay rates in different compounds on the refractive index n favours the virtual-cavity models [28]. According to this model, χ equals to $n[(n^2+2)/3]^2$.

In the same paper, Duan *et al* also simplified equation (4) with approximations for the 5d $\rightarrow$ 4f emission of Ce^{3+} ions and the total spontaneous emission rate of the 5d $\rightarrow$ 4f Ce^{3+} emission is given by [28]:

$$\Gamma_r = \frac{1}{\tau_r} = \frac{64\pi^4 e^2}{5h}\left(\frac{n(n^2+2)}{3}\right)^2 |\langle 5d|r|4f\rangle|_{eff}^2 \overline{v}^3 \tag{5}$$

where τ_r is the radiative lifetime, $\overline{v}$ is the average wavenumber, n is the refractive index, and $|\langle 5d|r|4f\rangle|_{eff}$ is the effective electric dipole radial integral between 4f and 5d orbitals. For the Ce^{3+} free ion, $|\langle 5d|r|4f\rangle|_{eff}$ is 0.025 nm [29].

The lifetimes τ_r, peak wavelengths of emission spectra λ, and refractive indices n of Ce^{3+} in REX_3 (RE = La, Pr and X = Cl, Br) are summarized in table 2. Unfortunately, there is no information on the refractive index for $PrCl_3$ and $PrBr_3$. With the known values of n for $LaCl_3$ and $LaBr_3$, we obtain $|\langle 5d|r|4f\rangle|_{eff} = 0.031$ nm; see column 4 in table 2. This value is larger than the free ion value of 0.025 nm, contrary to the expectation in [30] that it should be smaller than the free ion value. Duan *et al* obtained $|\langle 5d|r|4f\rangle|_{eff}$ varying between 0.022 and 0.034 nm

with an average of 0.028 nm from the data of various hosts and concluded that the values of Ce^{3+} effective radial integral $|\langle 5d|r|4f\rangle|_{eff}$ are larger in crystals than in vacuum [28].

From the data of $|\langle 5d|r|4f\rangle|_{eff}$ of various hosts, we assume that the values of $|\langle 5d|r|4f\rangle|_{eff}$ for $PrCl_3$ and $PrBr_3$ should fall between 0.022 and 0.034. With these values, we calculate the ranges of the refractive indices for $PrCl_3$ and $PrBr_3$ as shown in column 5 of table 2. Table 2 shows that the decay times excited via the Ce^{3+} 5d state at 10 K of $PrCl_3$:Ce^{3+} and $PrBr_3$:Ce^{3+} are not inconsistent with the spontaneous radiative emission rates derived from equation (4). However, there is also a possibility that the Ce^{3+} emission is already quenched even at very low temperature.

4.2. Quenching mechanisms of Ce^{3+} emission

The 5d $\rightarrow$ 4f radiative emission process is often highly efficient. Multiphonon relaxation between the 5d and 4f states is usually unimportant because of the large energy separation between the 5d and 4f states. Nevertheless, the Ce^{3+} emission is found to be completely quenched in a number of hosts, such as Y_2O_3, La_2O_3, and La_2O_2S [32]. Our results show that Ce^{3+} emission is thermally quenched in $PrBr_3$:Ce^{3+} with an activation energy of 0.15 eV; see figure 7. Several explanations have been put forward to explain the Ce^{3+} quenching luminescence. These include the thermally excited interconfigurational system crossing from 5d to 4f of Ce^{3+}, Förster–Dexter energy transfer from Ce^{3+} to nearby centres, electron transfer and photoionization [32].

In the first case, the parabola offset can be estimated from the Stokes shift of the Ce^{3+} emission. As far as we are aware, this Stokes shift is never large enough to explain Ce^{3+} luminescence quenching of the Ce^{3+} ion [32]. In the second case, the Ce^{3+} ion loses its excitation energy by nonradiative energy transfer to nearby centres [33]. A high transfer rate requires an overlap between the emission spectrum of Ce^{3+} with the absorption spectrum of the other centre. This type of transfer is well known in Ce^{3+}-doped Gd^{3+}-based compounds [34]. In the third case, the electron in the 5d state of Ce^{3+} is promoted to one of its nearest or next-nearest neighbors. In the last case, the 5d electron of the excited Ce^{3+} ion is promoted into the conduction band because of the proximity of the lowest 5d excited state of Ce^{3+} to the conduction band. The activation energy is then related to the energy difference between the lowest 5d Ce^{3+} state and the host conduction band. This thermal quenching was previously observed in some Ce^{3+}-doped oxides [35]. Recently, the absence of Ce^{3+} luminescence at RT in LaI_3:Ce^{3+} was also attributed to this thermal quenching [36].

For $PrBr_3$:Ce^{3+}, the thermally excited interconfigurational system crossing from 5d to 4f of Ce^{3+} is not possible. The Stokes shift of the Ce^{3+} emission in $PrBr_3$:Ce^{3+} of 0.61 eV is similar to the 0.54 eV of $LaBr_3$:Ce^{3+}; see figures 3 and 4. Additionally, $LaBr_3$:Ce^{3+} does not show the Ce^{3+} luminescence quenching. The Förster–Dexter energy transfer from Ce^{3+} to nearby centres is also not possible in $PrBr_3$:Ce^{3+}. There is no overlap between the 5d $\rightarrow$ 4f Ce^{3+} emission and the $^3H_4 \rightarrow {}^3P_2$ excitation at 448 nm (2.77 eV). This leaves the electron transfer to neighbouring ions or the photoionization as possible quenching mechanisms.

In this work, we first estimate the position of the Ce^{3+} emitting level relative to the conduction and valence bands in $PrBr_3$:Ce^{3+}. Next, based on these level positions, we propose a model for the thermal quenching of Ce^{3+} luminescence in $PrBr_3$:Ce^{3+}.

4.3. Energy-level schemes in $LaBr_3$:Ce^{3+} and $PrBr_3$:Ce^{3+}

The energy-level scheme of $PrBr_3$:Ce^{3+} is shown in figure 8. The scheme has been constructed with the information on the host lattice excitations, 4f $\rightarrow$ 5d excitations, and Pr^{3+} CT excitation

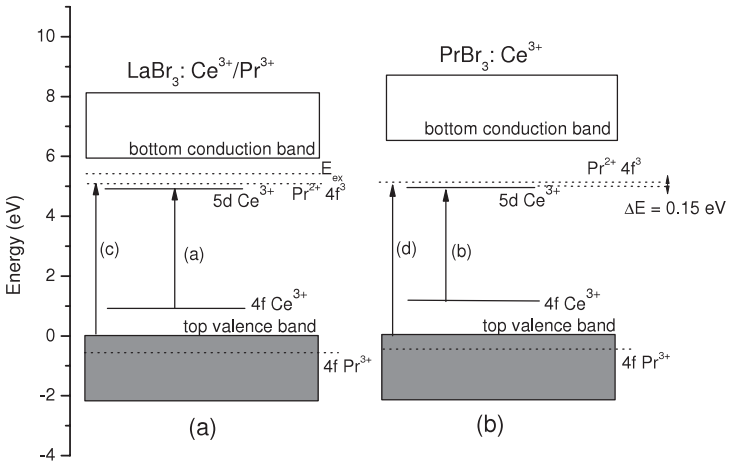

Figure 8. Energy-level schemes of (a) $LaBr_3$:Ce^{3+}/Pr^{3+} and (b) $PrBr_3$:Ce^{3+}.

energy. The scheme for $LaBr_3$:Ce^{3+} taken from Dorenbos *et al* is also presented [6]. The top of the bromide valence band is defined as the zero of energy. The bottom of the conduction bands (E_{VC}) of $LaBr_3$ and $PrBr_3$ is located at 5.90 ± 0.15 and 6.50 ± 0.15 eV, respectively. Arrows (a) and (b) indicate the energy differences (E_{fd}) between the lowest 4f and lowest 5d states of Ce^{3+} in $LaBr_3$ and $PrBr_3$, respectively.

Arrows (c) and (d) indicate the observed energy for CT from bromide to Pr^{3+} in $LaBr_3$ and $PrBr_3$ of 5.00 and 5.17 eV, respectively. The Pr^{3+} CT energies in $LaBr_3$ and $PrBr_3$ were obtained from [6] and the excitation spectrum (f) in figure 3, respectively. After CT, Pr^{3+} is converted to Pr^{2+} and the transferred electron is located in the $4f^3$ ground state of Pr^{2+}.

In $LaBr_3$, the 4f ground state of Ce^{3+} is located at 0.90 ± 0.40 eV above the top of the valence band [6]. This value, together with E_{fd}, locates the lowest 5d state of Ce^{3+} at 4.93 ± 0.40 eV above the valence band, which is close to the location of the $4f^3$ ground state of Pr^{2+} in $LaBr_3$. The lowest 5d state of Ce^{3+} in $LaBr_3$ is at ∼1 eV below the bottom of the conduction band. This large energy difference is consistent with the absence of Ce^{3+} emission quenching in $LaBr_3$ even at a temperature of 600 K [18]. We expect that the location of the 4f ground state of Ce^{3+} in $PrBr_3$ is not too much different from that in $LaBr_3$, since both lattices share the same structure with similar lattice parameters. We also expect that the 4f ground state of Pr^{3+} in $PrBr_3$ should not be too much different than that in $LaBr_3$:Pr^{3+}. The 4f ground state of Pr^{3+} in $LaBr_3$:Pr^{3+} is located at 0.61 ± 0.40 eV below the top of valence band [6]. We then arrive at a scheme shown in figure 8(b), which is very similar to that of $LaBr_3$.

From this energy-level scheme, the distance between the Ce^{3+} lowest 5d excited state to the host conduction band is much larger than the 0.15 ± 0.01 eV thermal activation energy found in figure 7. Therefore the thermal quenching of luminescence in $PrBr_3$:Ce^{3+} cannot be explained by ionization of the 5d electron to the conduction band.

4.4. A model for the thermal luminescence quenching

We propose a new model for the thermal luminescence quenching in $PrBr_3$:Ce^{3+} that is based on electron transfer from Ce^{3+} to Pr^{3+}. Such transfer in solids is usually referred to as metal-to-metal CT or intervalence CT [37]. The model is shown schematically in figure 9.

On excitation of the Ce^{3+} 5d states at low temperature of 10 K, we have ordinary Ce^{3+} 5d → 4f emission. When the temperature increases, thermal energy (ΔE) of

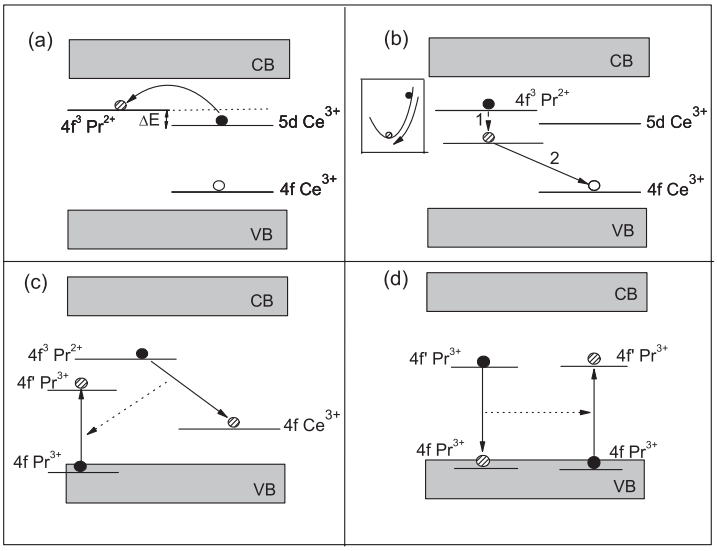

Figure 9. Schematic representation of the proposed model relating the thermal luminescence quenching in $PrBr_3$:Ce^{3+}. CB and VB are the conduction band and the valence band, respectively. The schemes are ordered alphabetically.

0.15 ± 0.01 eV is provided to the electron in the Ce^{3+} excited 5d configuration. Since the Ce^{3+} 5d state is close in energy to the empty $4f^3$ state of Pr^{2+}, the 5d electron can transfer to the empty $4f^3$ state of Pr^{2+}; see part (a) in figure 9. This is a metal-to-metal CT of the form:

$$(Ce^{3+})_{5d} + Pr^{3+} \rightarrow Ce^{4+} + Pr^{2+}. \tag{6}$$

After CT, Ce^{4+} and Pr^{2+} are created and substantial lattice relaxation occurs; see arrow 1 in part (b) of figure 9. A large lattice relaxation in Pr^{2+} is shown by the inset in part (b) of figure 9. The electron in the relaxed $4f^3$ state of Pr^{2+} cannot return to the Ce^{3+} 5d state and jumps back to the ground state of Ce^{3+}. This process is indicated by arrow 2.

The energy of the recombination of the electron in the $4f^3$ state of Pr^{2+} and the hole in the ground state of Ce^{4+} leaves Pr^{3+} in an excited state; see part (c) in figure 9. The excited Pr^{3+} relaxes, resulting in $4f^2 \rightarrow 4f^2$ emission. This corresponds to the presence of the Pr^{3+} $4f^2 \rightarrow 4f^2$ transition lines at RT in the emission spectrum of $PrBr_3$:Ce^{3+} excited at the Ce^{3+} $4f \rightarrow 5d$ excitation band; see spectrum (c) in figure 4:

$$Pr^{2+} + Ce^{4+} \rightarrow (Ce^{3+})_{gs} + Pr^{3+*} \tag{7}$$

$$Pr^{3+*} \rightarrow Pr^{3+} + h\nu. \tag{8}$$

From the same emission spectrum, we observe that the intensity of the Pr^{3+} $4f^2 \rightarrow 4f^2$ emission lines is weak. This can be explained by part (d) in figure 9. This figure shows an energy transfer from one Pr^{3+} ion to its neighbouring Pr^{3+} ion. The excitation can migrate through the lattice until it meets a killer site and is then lost for luminescence. This phenomenon is often called concentration quenching. This quenching is indicated by the decrease of the decay time of Pr^{3+} $4f^2 \rightarrow 4f^2$ emission when the Pr^{3+} concentration increases, as reported previously by German and Kiel in $LaCl_3$:Pr^{3+} and $LaBr_3$:Pr^{3+} [11].

We did not observe a shortening of the decay time of the 5d state of Ce^{3+} in $PrCl_3$ when the temperature increases from 10 K to RT; see curves (a) in figure 5. Apparently, the energy difference between the lowest 5d state of Ce^{3+} and the $4f^3$ ground state of Pr^{2+} in $PrCl_3$ is larger than in $PrBr_3$.

The scintillation light yield of $PrCl_3$:Ce^{3+} in table 1 is 42% of that of $LaCl_3$:Ce^{3+}. The low light yield cannot be attributed to thermal quenching of Ce^{3+} emission, since that was not observed. Additionally, the light yield at $T = 0$ K for $PrBr_3$:Ce^{3+} of 28 100 $\pm$ 300 photons MeV^{-1} is also 42% of the light yield for $LaBr_3$:Ce^{3+}; see figure 7 and table 1. Both low light yields in $PrCl_3$:Ce^{3+} at RT and $PrBr_3$:Ce^{3+} at $T = 0$ K can be due to the less efficient energy transfer towards Ce^{3+} centre via energy migration over the $5d_1$ state of Pr^{3+}, as reported previously in PrF_3:Ce^{3+} [7].

5. Conclusion

We have investigated the scintillation properties and the luminescence characteristics of $PrCl_3$:Ce^{3+} and $PrBr_3$:Ce^{3+}. The scintillation light yield and the optically luminescence decay time of $PrBr_3$:5% Ce^{3+} are thermally quenched with an activation energy of 0.15 $\pm$ 0.01 eV. A model of thermal luminescence quenching based on electron transfer from Ce^{3+} to Pr^{3+} has been proposed. We conclude that the thermal activation energy is related to the energy difference between the $4f^3$ state of Pr^{3+} and the lowest 5d state of Ce^{3+}. However, the Ce^{3+} emission quenching was not observed in $PrCl_3$:Ce^{3+}. This is due to the larger energy difference between the lowest 5d state of Ce^{3+} and the $4f^3$ ground state of Pr^{2+} in $PrCl_3$ compared to that in $PrBr_3$.

Acknowledgments

These investigations have been supported by the Netherlands Technology Foundation (STW), the Swiss National Science Foundation, the European Community Research Infrastructure Action under the FP6 'Structuring the European Research Area' Programme (through the Integrated Infrastructure Initiative 'Integrating Activity on Synchrotron and Free Electron Laser Science') and Saint Gobain, crystals and detectors division, Nemours, France.

References

[1] Guillot-Noël O, de Haas J T M, Dorenbos P, van Eijk C W E, Krämer K W and Güdel H U 1999 *J. Lumin.* **85** 21
[2] van Loef E V D, Dorenbos P, van Eijk C W E, Krämer K W and Güdel H U 2001 *Appl. Phys. Lett.* **79** 1573
[3] Shah K S, Glodo J, Klugerman M, Higgins W, Gupta T, Wong P, Moses W W, Derenzo S E, Weber M J and Dorenbos P 2004 *IEEE Trans. Nucl. Sci.* **51** 2302
Birowosuto M D, Dorenbos P, van Eijk C W E, Krämer K W and Güdel H U 2005 *IEEE Trans. Nucl. Sci.* **52** 1114
Birowosuto M D, Dorenbos P, van Eijk C W E, Krämer K W and Güdel H U 2006 *J. Appl. Phys.* **99** 123520
[4] Nikl M, Ogino H, Krasnikov A, Beitlerova A, Yoshikawa A and Fukuda T 2005 *Phys. Status Solidi* a **202** R4
Nikl M, Ogino H, Yoshikawa A, Mihokova E, Pejchal J, Beitlerova A, Novoselov A and Fukuda T 2005 *Chem. Phys. Lett.* **410** 218
[5] Dorenbos P 2002 *Nucl. Instrum. Methods Phys. Rev.* A **486** 208
[6] Dorenbos P, van Loef E V D, Vink A J P, van der Kolk E, van Eijk C W E, Krämer K W, Güdel H U, Higgins W M and Shah K 2006 *J. Lumin.* **117** 147
[7] Nikl M, Yoshikawa A, Satonaga T, Kamada K, Sato H, Solovieva N, Beitlerova A and Fukuda T 2004 *Phys. Status Solidi* a **201** R108
[8] Birowosuto M D, Dorenbos P, van Eijk C W E, Krämer K W and Güdel H U 2006 *IEEE Trans. Nucl. Sci.* **53** 3028
[9] Varsanyi F 1971 *Appl. Phys. Lett.* **19** 169
[10] German K R, Kiel A and Guggenheim H 1973 *Appl. Phys. Lett.* **22** 87
German K R and Kiel A 1974 *Phys. Rev. Lett.* **33** 1039
[11] German K R and Kiel A 1973 *Phys. Rev.* B **8** 1846
German K R, Kiel A and Guggenheim H 1975 *Phys. Rev.* B **11** 2436

[12] Reed J B, Hopkins B S and Audrieth L F 1936 *Inorg. Synth.* **1** 28
Meyer G 1989 *Inorg. Synth.* **25** 146
[13] Schmid B, Hälg B, Furrer A, Urland W and Kremer R 1987 *J. Appl. Phys.* **61** 3426
[14] de Haas J T M, Dorenbos P and van Eijk C W E 2005 *Nucl. Instrum. Methods Phys. Rev.* A **537** 97
[15] Bollinger L M and Thomas G E 1961 *Rev. Sci. Instrum.* **32** 1044
[16] Zimmerer G 1993 *Nucl. Instrum. Methods Phys. Rev.* A **336** 253
[17] Birowosuto M D, Dorenbos P, van Eijk C W E, Krämer K W and Güdel H U 2006 *J. Phys.: Condens. Matter* **18** 6133
[18] Bizarri G, de Haas J T M, Dorenbos P and van Eijk C W E 2006 *Phys. Status Solidi* a **203** R41
[19] van Loef E V D, Dorenbos P, van Eijk C W E, Krämer K W and Güdel H U 2001 *IEEE Trans. Nucl. Sci.* **48** 341
[20] van Loef E V D, Dorenbos P, van Eijk C W E, Krämer K W and Güdel H U 2003 *Phys. Rev.* B **68** 045108
[21] Hargreaves W A 1992 *J. Phys.: Condens. Matter* **4** 6141
[22] Dorenbos P 2000 *J. Lumin.* **91** 91
[23] Dorenbos P 2005 *Chem. Mater.* **17** 6452
[24] Dorenbos P 2000 *Phys. Rev.* B **62** 15640
[25] Andriessen J, Antonyak O T, Dorenbos P, Rodnyi P A, Stroganyuk G B, van Eijk C W E and Voloshinovskii A S 2000 *Opt. Commun.* **178** 355
[26] Totygin D 2003 *J. Flouresc.* **13** 201
[27] Berman P R and Milonni P W 2004 *Phys. Rev. Lett.* **92** 053601
[28] Duan C K and Reid M F 2006 *Curr. Appl. Phys.* **6** 348
[29] Duan C K and Reid M F 2005 *J. Chem. Phys.* **122** 094714
[30] Krupke W F 1966 *Phys. Rev.* **145** 325
[31] Dorenbos P 2006 *Radiation Detectors for Medical Applications* ed S Tavernier, A Gektin, B Grinyov and W W Moses (Berlin: Springer) p 195
[32] Blasse G, Schipper W and Hamelink J J 1991 *Inorg. Chim. Acta* **189** 77
[33] Förster Th 1948 *Ann. Phys., Lpz.* **2** 55
Dexter D L 1953 *J. Chem. Phys.* **21** 836
[34] de Vries A J, Smeets W J J and Blasse G 1987 *Mater. Chem. Phys.* **18** 81
Schaart D R, Dorenbos P, van Eijk C W E, Visser R, Pedrini C, Moine B and Khaidukov N M 1995 *J. Phys.: Condens. Matter* **7** 3063
van Loef E V D, Dorenbos P, van Eijk C W E, Krämer K W and Güdel H U 2001 *Opt. Commun.* **189** 297
[35] Kappers L A, Bartram R H, Hamilton D S, Lempicki A and Glodo J 2003 *J. Lumin.* **102/103** 162
Jia D, Wang X and Yen W M 2004 *Phys. Rev.* B **69** 235113
van der Kolk E, Dorenbos P, de Haas J T M and van Eijk C W E 2005 *Phys. Rev.* B **71** 045121
van der Kolk E, Dorenbos P, van Eijk C W E, Basun S A, Imbusch G F and Yen W M 2005 *Phys. Rev.* B **71** 165120
[36] Bessiere A, Dorenbos P, van Eijk C W E, Krämer K W and Güdel H U 2005 *Nucl. Instrum. Methods Phys. Rev.* A **537** 22
[37] Blasse G 1976 *Struct. Bond.* **26** 43
Blasse G 1991 *Struct. Bond.* **76** 153